Supporting Information

MOFs-derived N doped CoNi@C as Bifunctional Catalysts for Efficient Water Splitting

Xihui Yang, Zekun Li, Zikun Yang, Dapeng Meng and Zhao Wang *

National Engineering Research Centre of Industry Crystallization Technology, School of Chemical Engineering and Technology, Tianjin University, Tianjin 300072, China

*E-mail address: wangzhao@tju.edu.cn

DFT calculation method:

The calculations carried out in this work were based on density functional theory (DFT) and the projector augmented wave (PAW) method. Exchange-correlation interactions were modeled using the generalized gradient approximation with the Perdew–Burke–Ernzerhof (GGA-PBE) functional, as implemented in the Vienna ab initio simulation package (VASP).[1-5] The calculations were performed using a cutoff energy of 500eV, and Fermi-level smearing of 0.05 was applied. A G-centered 6× 6× 6 and 14× 14× 14 was used for bulk calculations of CoN and Co cell, respectively (Figure S18). After extracting Co_3N_3 clusters from the CoN unit cell and further optimizing their geometry, the Co_3N_3 clusters form a CoN/Co heterostructure with Co (111) (Figure S19). Subsequently, 5 Co atoms in Co (111) were replaced with nickel to approximate the nickel-cobalt ratio in Ni_1Co_{10} (1:9.3). While 3 × 3 × 1 used for slabs calculations for CoN/Ni_1Co_{10}. The convergence criterion for total energy and Hellmann-Feynman forces were set to be 1×10^{-5} eV and 0.04 eV/Å. Spin polarization and dipole corrections were considered in all calculations.[6,7] The periodic slabs included 5 layers of atoms and a 15 Å thick vacuum layer, and constraint the bottom layer atoms and relax the top 4 layers of atoms on the surface. The free energy of intermediate structure was obtained by processing the result of frequency calculation using VASPKIT.[8]

The adsorption energy of intermediate on the catalyst surface could be calculated by the following equations:

$$\Delta E_{ads}^{*} = E(ads^{*}) - E(*) - E(ads)$$

Where the * represented the active site of the catalyst surface, ads represented the intermediate, and ads* represented the intermediate adsorbed on the active site of the catalyst

The free energy of intermediate adsorption was calculated by the following equations:

$$\Delta G_{ads} = \Delta E_{ads} + \Delta E_{ZPE} + \Delta U_{(0\rightarrow T)} - T\Delta S \text{ [8]}$$

Where ΔG_{ads} represented the free energy of intermediate. The $\Delta E_{ZPE} + \Delta U_{(0\rightarrow T)} - T\Delta S$ was obtained by VASPKIT processing the result of frequency calculation (Table S5 and S6)[8]

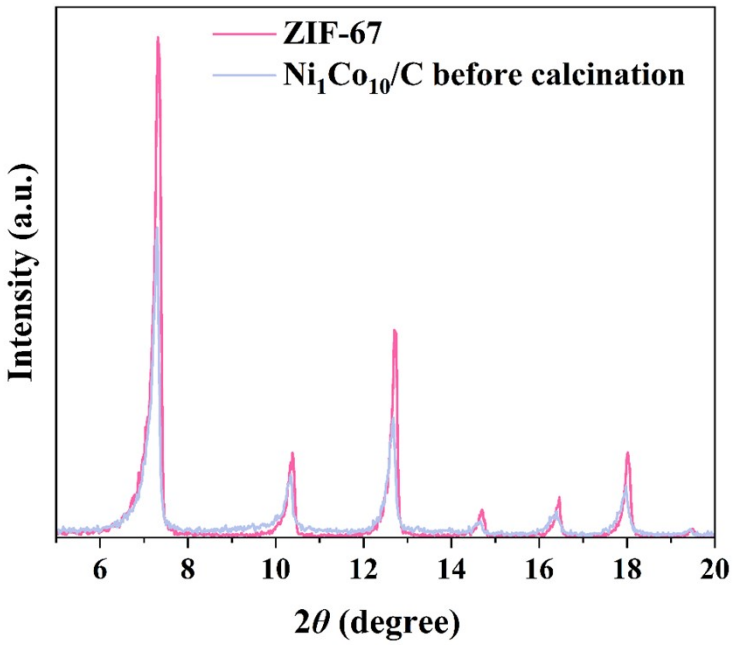

Figure S1. XRD spectra of ZIF-67 and Ni_1Co_{10}/C before calcination.

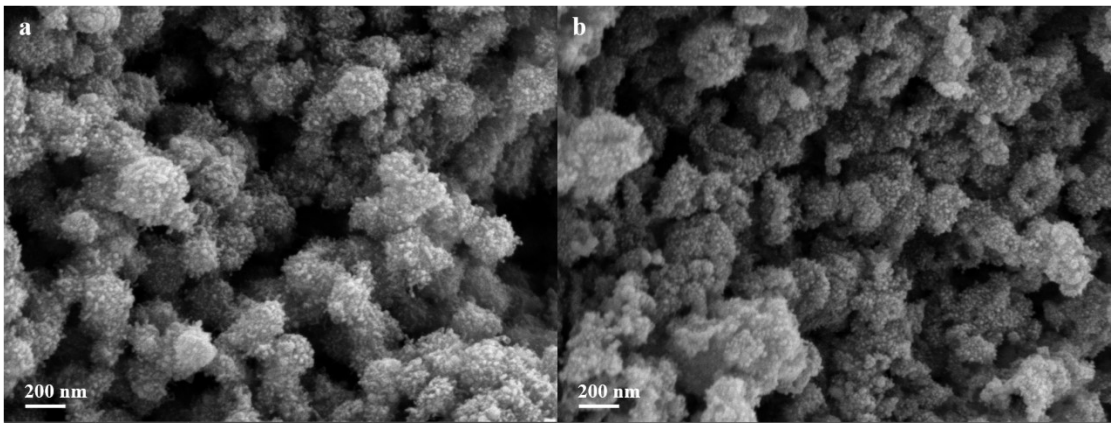

Figure S2. SEM images of (a) Co/C, (b) Ni_1Co_4/C.

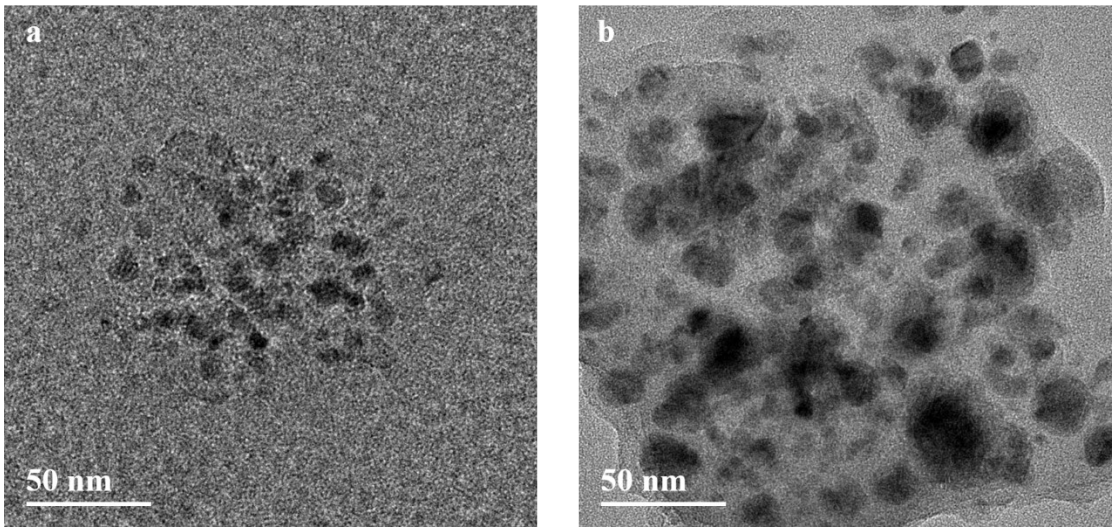

Figure S3. TEM images of (a) Co/C, (b) Ni_1Co_4/C.

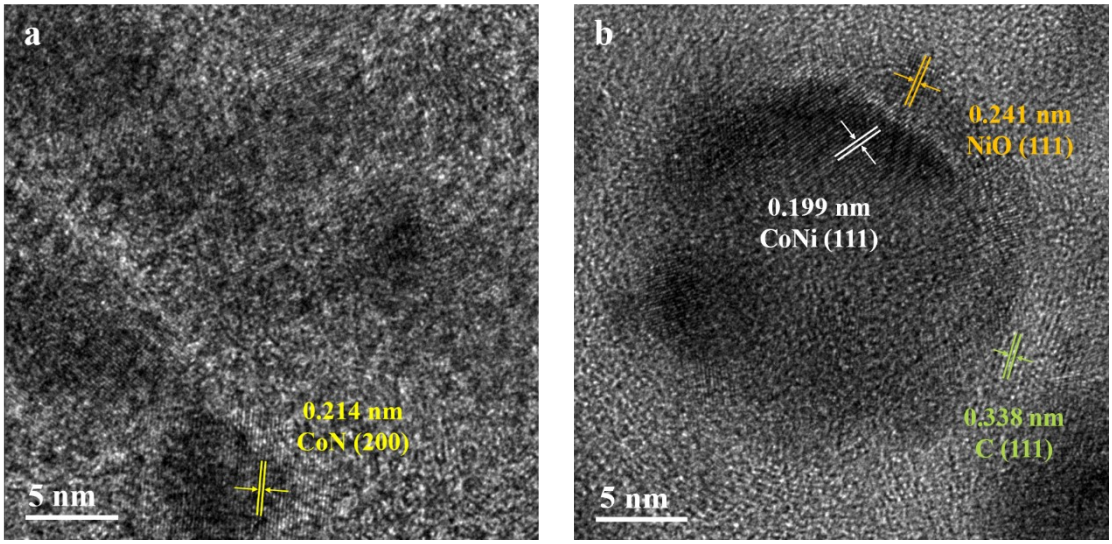

Figure S4. HRTEM images of (a) Co/C, (b) Ni_1Co_4/C.

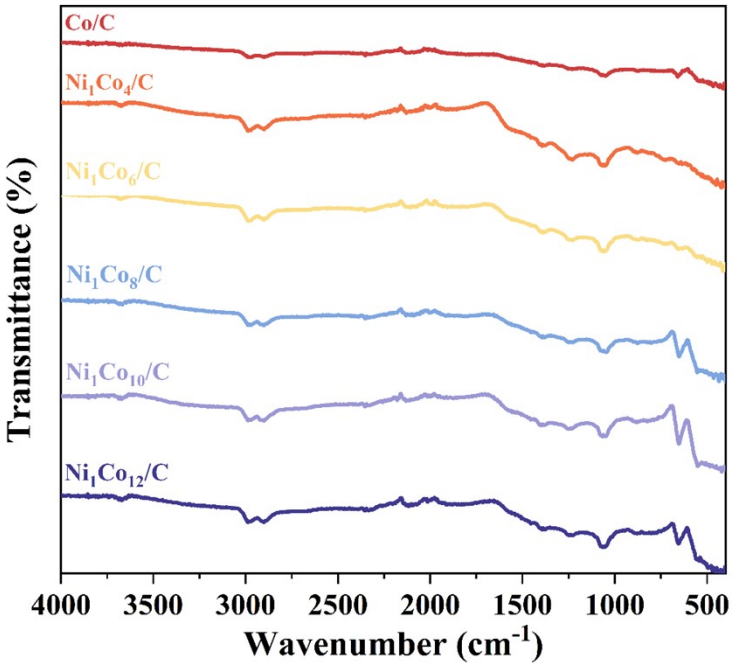

Figure S5. FTIR spectra of Co/C and Ni_1Co_X/C.

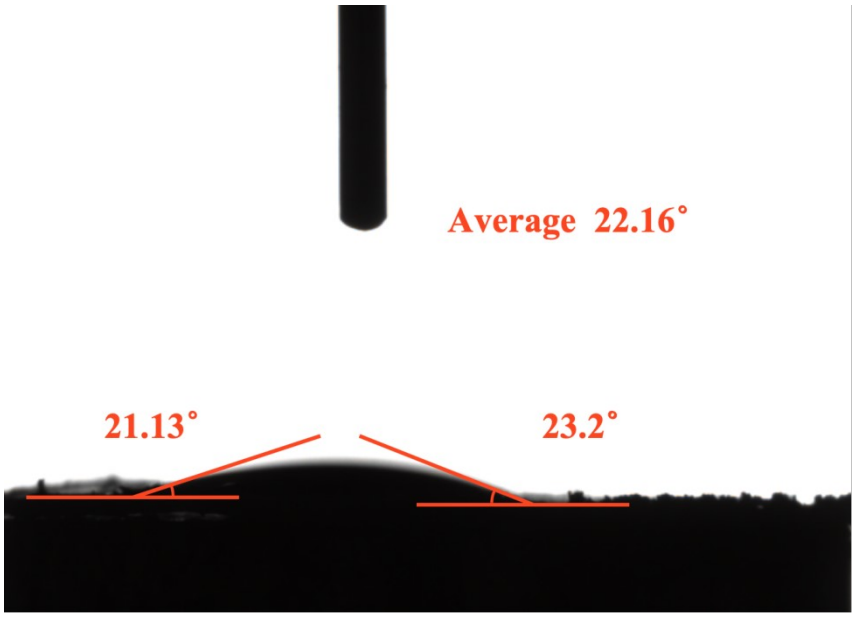

Figure S6. The contact angle of Ni_1Co_{10}/C and water.

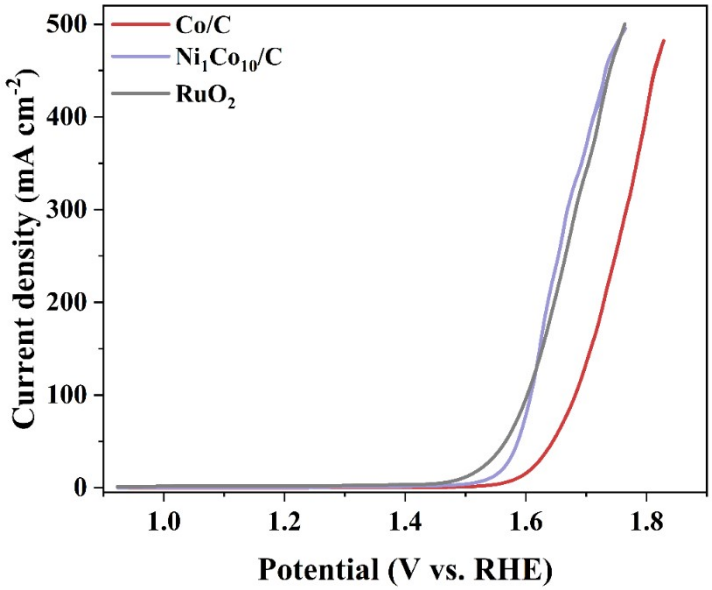

Figure S7. OER polarization curves of Co/C, Ni_1Co_{10}/C and RuO_2.

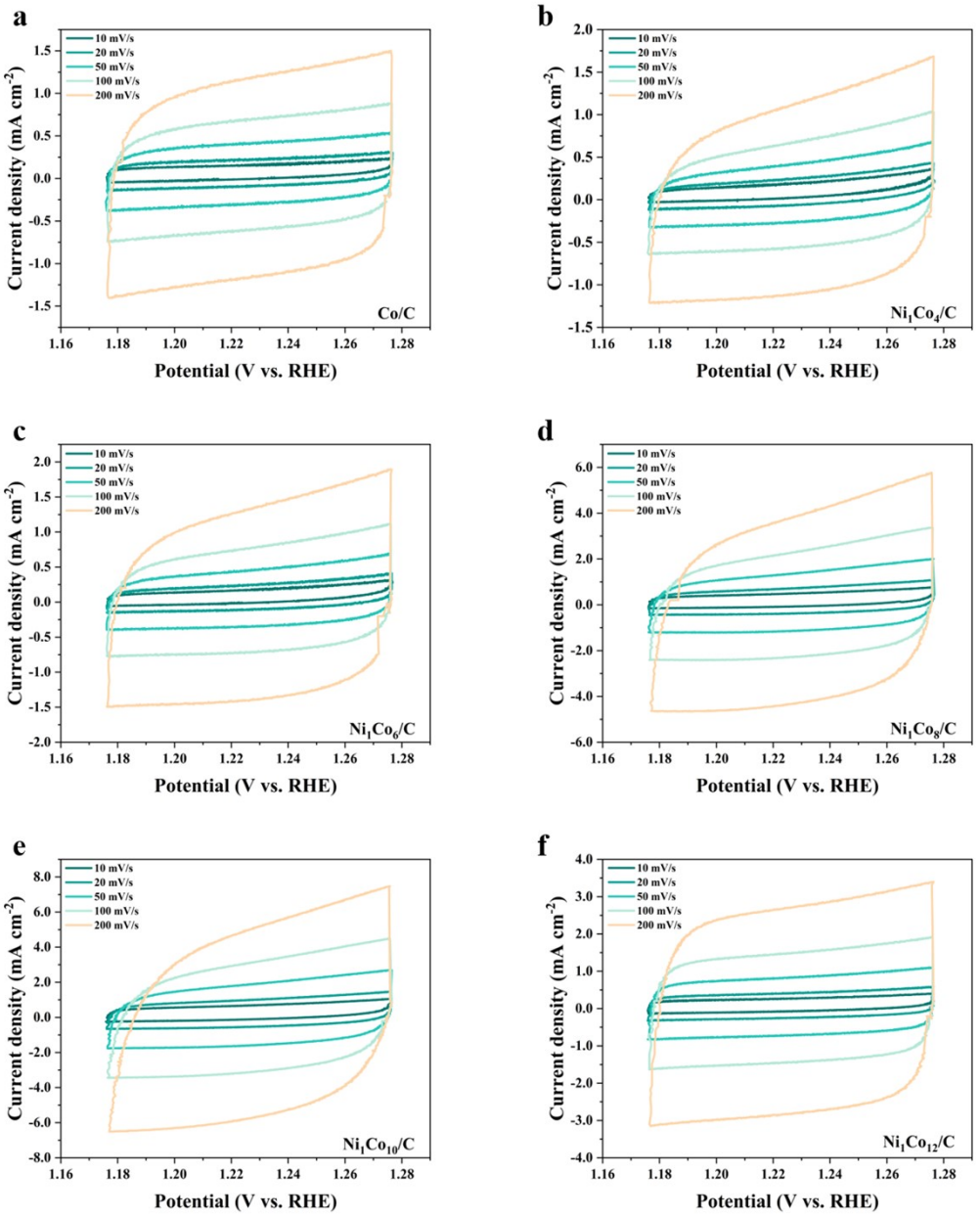

Figure S8. Cyclic voltammogram curves of (a) Co/C, (b) Ni_1Co_4/C, (c) Ni_1Co_6/C, (d) Ni_1Co_8/C, (e) Ni_1Co_{10}/C and (f) Ni_1Co_{12}/C at multiple scan rates (10, 20, 50, 100 and 200 mV s^{-1}).

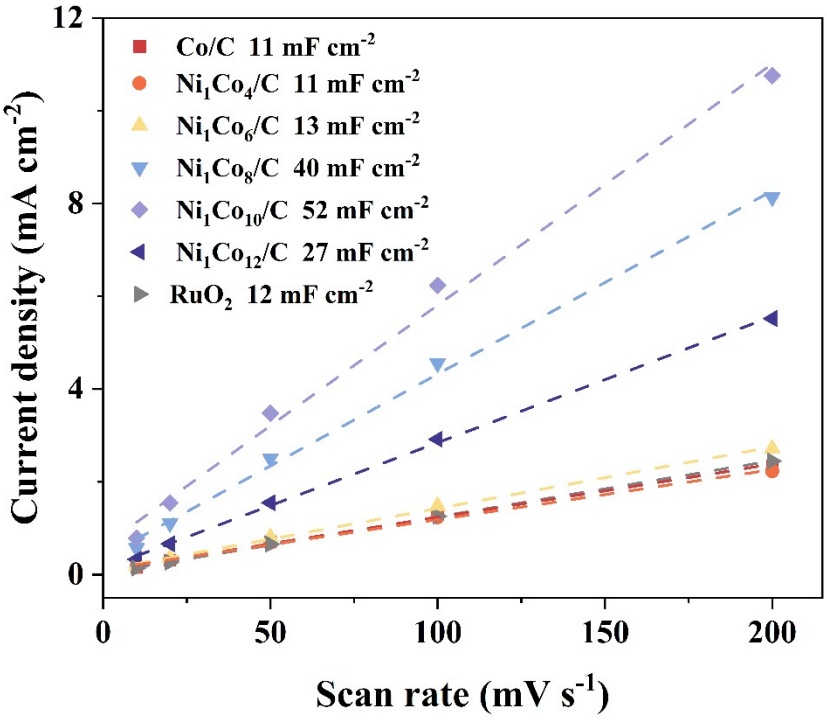

Figure S9. Double-layer capacitance of Co/C, Ni_1Cox/C (x = 4, 6, 8, 10, 12) and RuO_2.

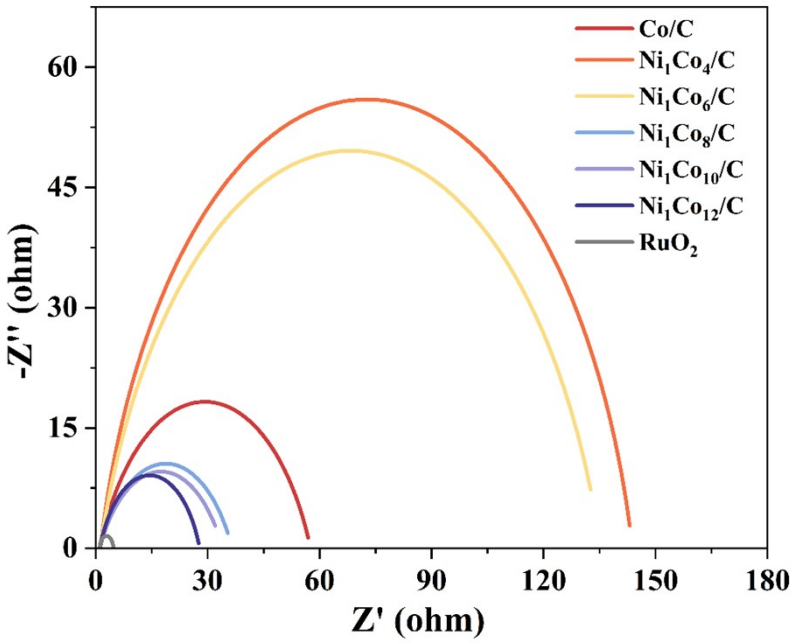

Figure S10. Electrochemical impedance spectroscopy (EIS) plots of OER of Co/C, Ni_1Cox/C (x = 4, 6, 8, 10, 12) and RuO_2.

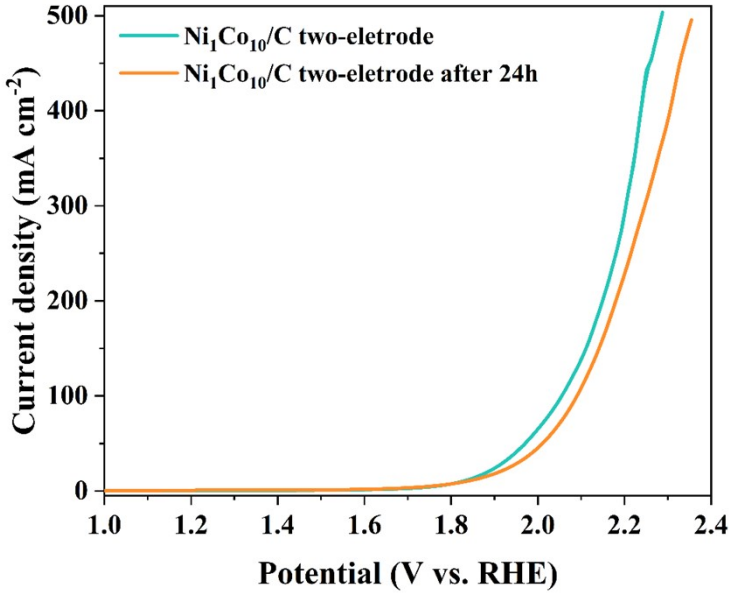

Figure S11. Bifunctional polarization curves of Ni_1Co_{10}/C before and after 24h stability test in double electrode system.

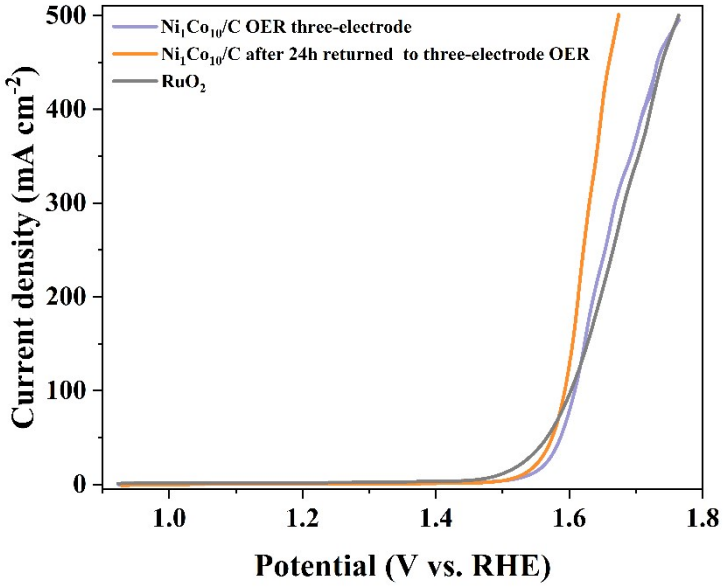

Figure S12. OER Polarization curves of Ni_1Co_{10}/C before and after 24h stability test.

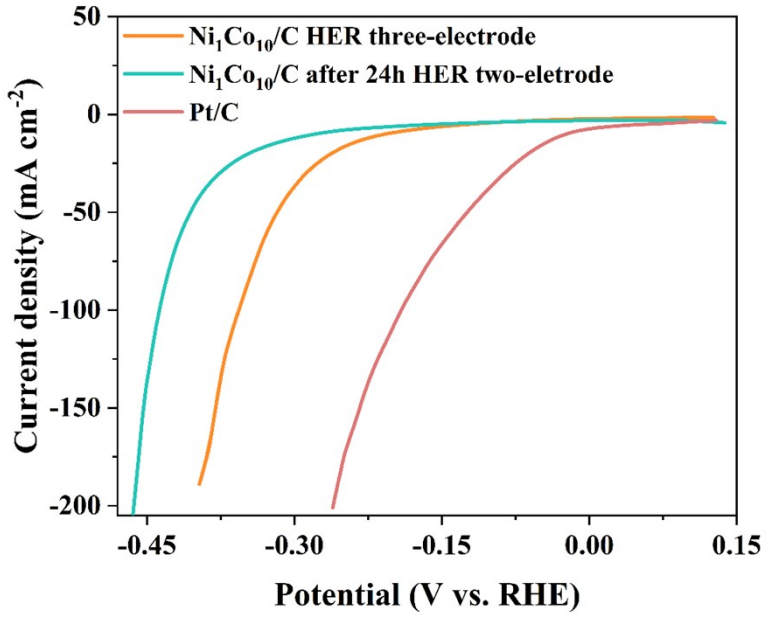

Figure S13. HER Polarization curves of Ni_1Co_{10}/C before and after 24h stability test.

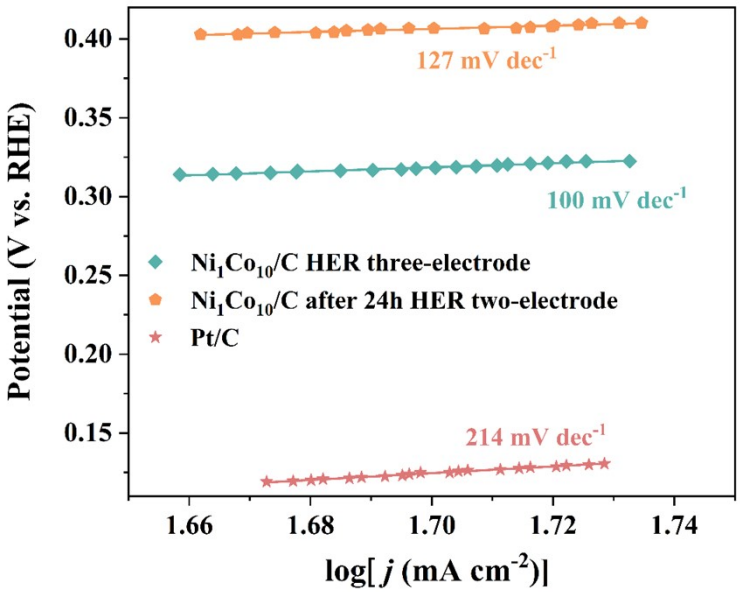

Figure S14. Tafel slope of Ni_1Co_{10}/C before and after 24h stability test.

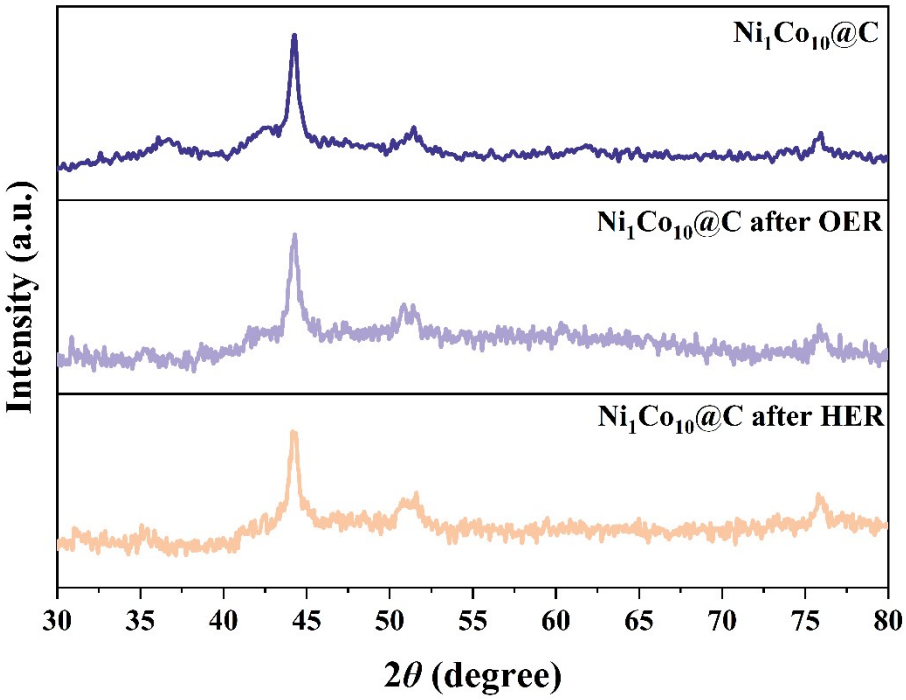

Figure S15. XRD of Ni_1Co_{10}/C before and after stability test.

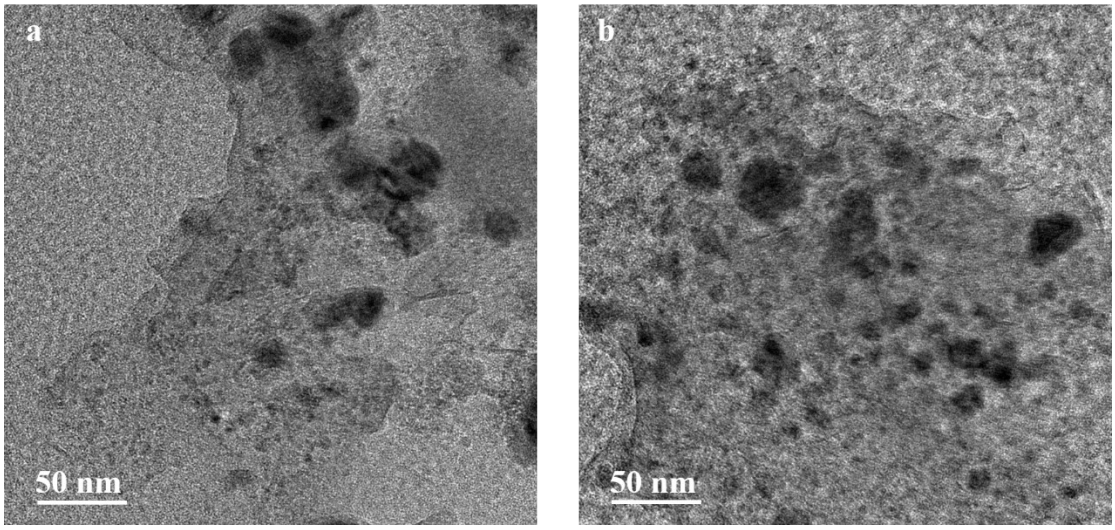

Figure S16. TEM of Ni_1Co_{10}/C before and after stability test.

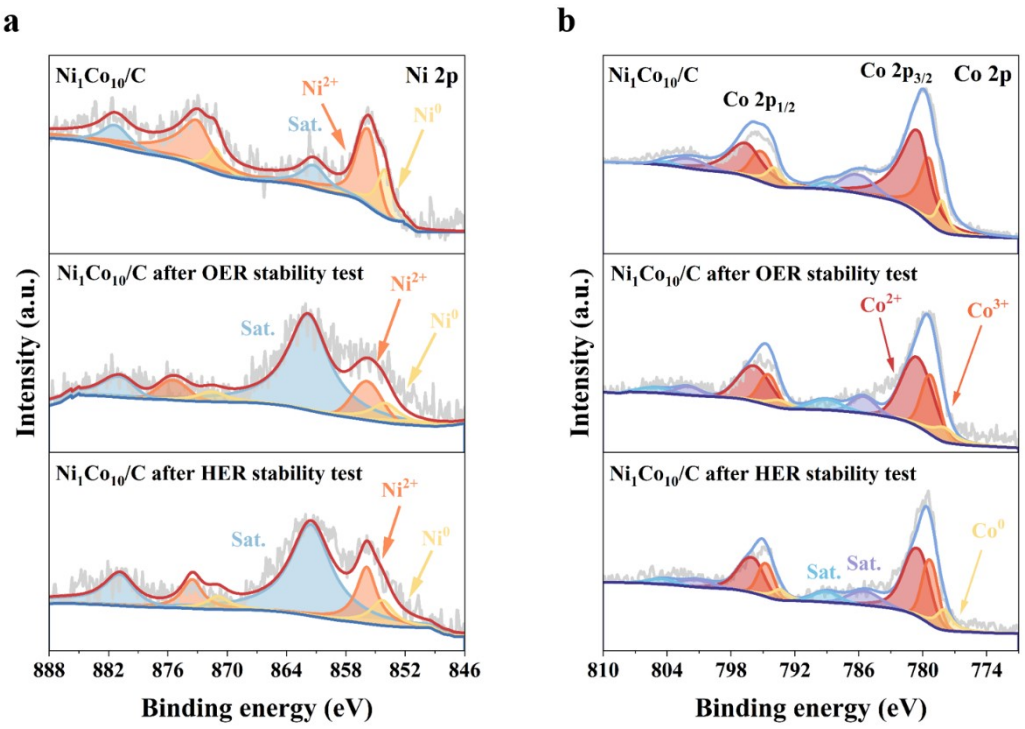

Figure S17. XPS of Ni_1Co_{10}/C before and after stability test.

The XRD of the Ni_1Co_{10}/C after the stability test are shown in Figure S15. No additional phases were observed, and the characteristic diffraction peaks remained unchanged compared to those before the stability test, indicating that the catalyst retained its structural integrity during the OER and HER processes, without any disruption to the spinel crystal structure. Similarly, the TEM results (Figure S16) confirmed this stability. The XPS spectra (Figure S17) of Co and Ni showed no shifts in the peaks, and the metal valence ratios remained largely unchanged, further supporting the excellent stability of the catalyst. (Note: due to the low catalytic dose on the carbon cloth after the reaction, the signal peaks are weak, and the satellite peaks are prominent.)

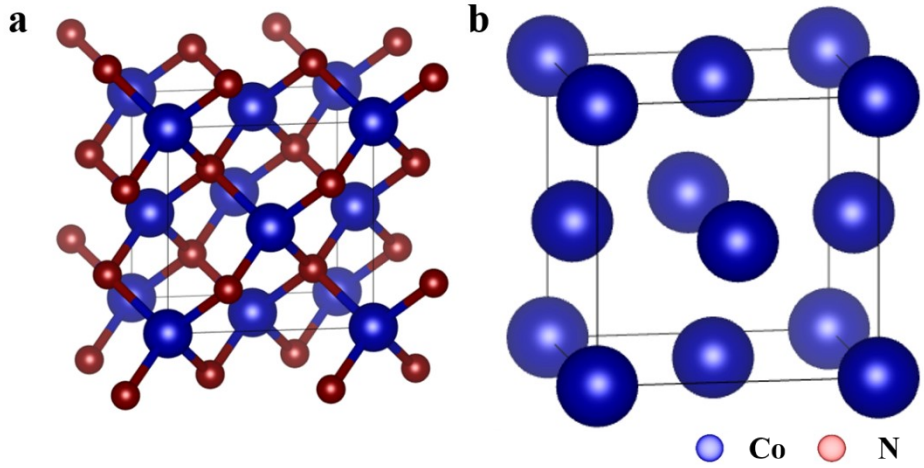

Figure S18. Atomic models of (a) CoN and (b) Co cell.

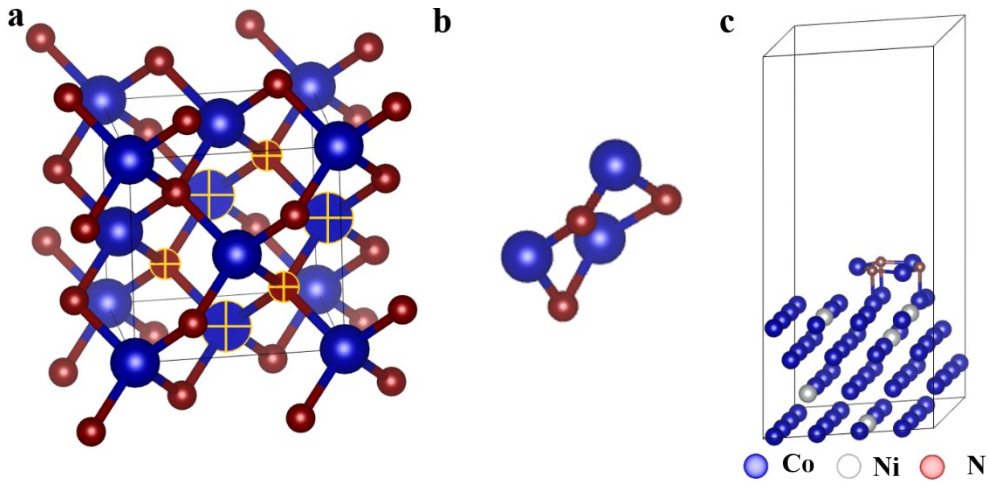

Figure S19. Atomic models of (a) Co_3N_3 clusters from CoN unit cell, (b) geometry optimized Co_3N_3 clusters and (c) CoN/CoNi heterostructure.

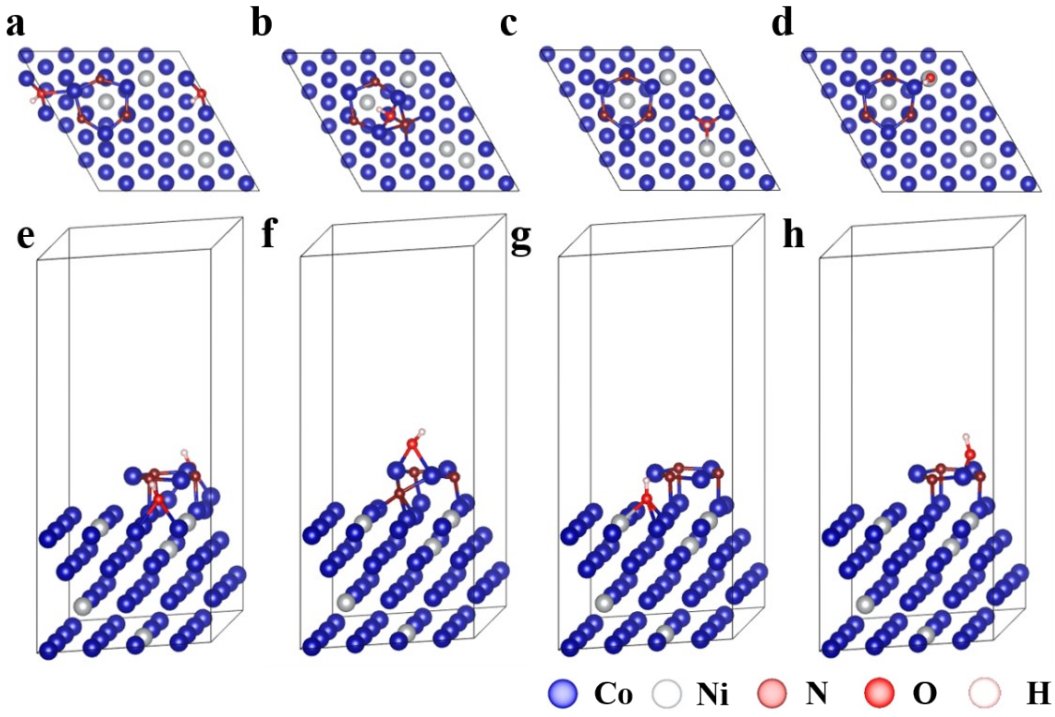

Figure S20. Atomic models from top vision of (a) (Co)CoN/CoNi(2Co), (b) (2Co)CoN/CoNi, (c) CoN/CoNi(2Co1Ni) and (d) (Co)CoN/CoNi about OH* adsorption. Atomic models from front vision of (e) (Co)CoN/CoNi(2Co), (f) (2Co)CoN/CoNi, (g) CoN/CoNi(2Co1Ni) and (h) (Co)CoN/CoNi about OH* adsorption. (CoN/CoNi stands for heterogeneous structure, the parentheses represent the active site for OH* adsorption in this model.)

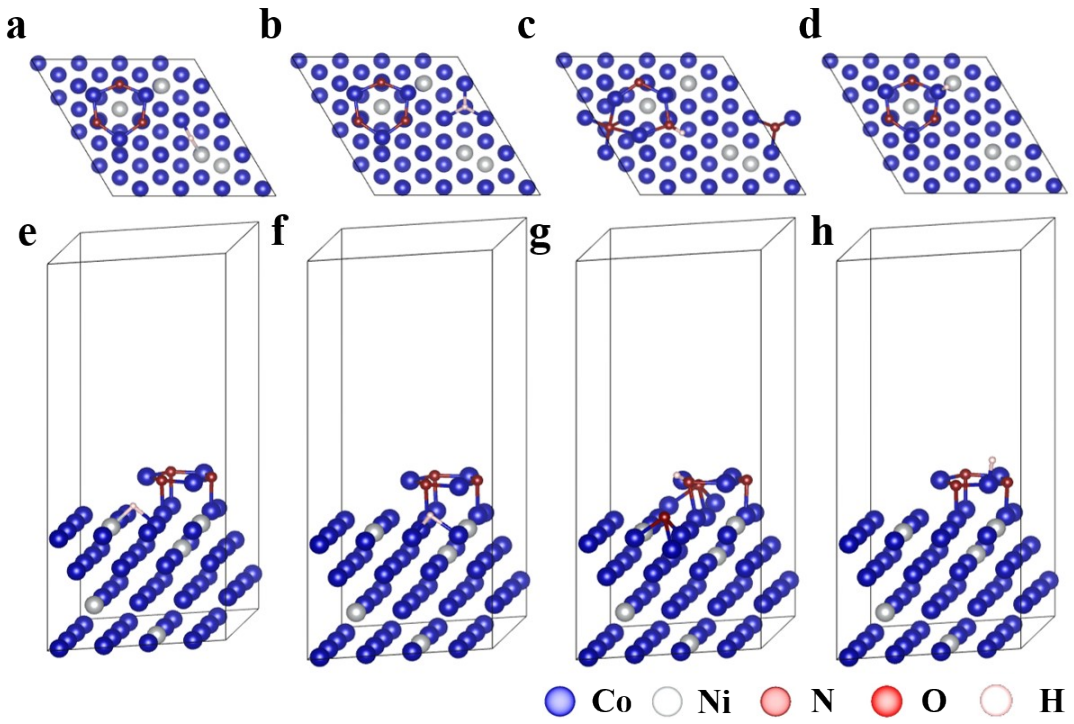

Figure S21. Atomic models from top vision of (a) CoN/CoNi(CoNi), (b) CoN/CoNi(3Co), (c) (N)CoN/CoNi and (d) (Co)CoN/CoNi about H* adsorption. Atomic models from front vision of (e) CoN/CoNi(CoNi), (f) CoN/CoNi(3Co), (g) (N)CoN/CoNi and (h) (Co)CoN/CoNi about H* adsorption. (CoN/CoNi stands for heterogeneous structure, the parentheses represent the active site for H* adsorption in this model.)

Table S1. XPS Relative Subpeak Area of N1s of Co/C, Ni_1Co_{10}/C and Ni_1Co_4/C.

Sample	Pyridinic N	Co/Ni-N_x	Pyrrolic N	Graphitic N	Oxidized N
Co/C	24.14%	34.74%	34.17%	6.63%	0.32%
Ni_1Co_{10}/C	20.86%	34.31%	30.07%	10.78%	3.98%
Ni_1Co_4/C	17.77%	47.39%	25.92%	8.14%	0.78%

Table S2. Specific surface area of the Co/C, Ni_1Co_{10}/C and Ni_1Co_4/C.

sample	S_{BET}/($m^2 \cdot g^{-1}$)	Pore Volume ($cm^3 \cdot g^{-1}$)
Co/C	210.79	0.234
Ni_1Co_{10}/C	190.85	0.263
Ni_1Co_4/C	158.87	0.255

Table S3. Comparison of the OER activity of the Ni_1Co_{10}/C with other electrocatalysts in 1 M KOH.

Catalysts	Overpotential (mV)	Tafel slope (mV dec^{-1})	Current density (mA cm^{-2})	Ref
Ni_1Co_{10}/C	380	53.9	100	Our work
NFO/NF	309	40	100	[9]
Ni_3N–CeO_2/NF	341	64.4	50	[10]
MnCoP/NF	415	76	100	[11]
Ni_3S_2@$FeNi_2S_4$@NF	379	92	100	[12]
MoS_2/Co−N−CN_2	398	/	10	[13]
CoOOH/Co_9S_8	360	86.4	100	[14]
Co 4mmol/NC	400	100	10	[15]
Co@bCNTs	330	113	10	[16]
DE-TDAP	346	67	10	[17]
Co_2P/Co_4N/CNTs	398	110	100	[18]

Table S4. Comparison of the HER activity of the Ni_1Co_{10}/C with other electrocatalysts in 1 M KOH.

Catalysts	Overpotential (mV)	Tafel slope (mV dec^{-1})	Current density (mA cm^{-2})	Ref
Ni_1Co_{10}/C	357	127	100	Our work
Ni_3N–CeO_2/NF	314	42.8	100	[10]
Fe/W-Ni_3S_2	253	102	50	[19]
Ni_5P_4/Ni_2P/Fe_2P-2	250	81.2	50	[20]
Co_3O_4–$CoFe_2O_4$@ MWCNT	342	138	100	[21]
$Ni_{0·5}Mo_{0.5}S_x$ + XC72R	402	81	100	[22]
Co_3O_4@MoO_3	158	148	10	[23]
Co/NC@PMDA	266	135.3	10	[24]

Table S5. Calculated $\Delta E_{ZPE} + \Delta U_{(0\rightarrow T)} - T\Delta S$ of OER.

Site	$\Delta E_{ZPE} + \Delta U_{(0\rightarrow T)} - T\Delta S$
(Co)CoN/CoNi(2Co)	0.321
(2Co)CoN/CoNi	0.349
CoN/CoNi(2Co1Ni)	0.316
(Co)CoN/CoNi	0.314

Table S6. Calculated $\Delta E_{ZPE} + \Delta U_{(0\rightarrow T)} - T\Delta S$ of HER.

Site	$\Delta E_{ZPE} + \Delta U_{(0\rightarrow T)} - T\Delta S$
CoN/CoNi(CoNi)	0.175
CoN/CoNi(3Co)	0.291
(N)CoN/CoNi	0.148
(Co)CoN/CoNi	0.160

References:

[1] G. Kresse and J. Hafner, *Phys. Rev. B*, 1993,47, 558-561.

[2] G. Kresse, J. Furthmüller, *Comp. mater. Sci.*, 1996, 6, 15-50.

[3] J. P. Perdew, K. Burke, M. Ernzerhof, *Phys. Rev. Lett.*, 1996, 77, 3865-3868.

[4] Blochl, *Phys. Rev. B*, 1994, 50, 17953-17979.

[5] G. Kresse, D. Joubert, *Phys. Rev. B*, 1999, 59, 1758-1775.

[6] S. Grimme, J. Antony, S. Ehrlich, H. Krieg, *J. Chem. Phys.*, 2010, 15, 132.

[7] S. Grimme, S. Ehrlich, L. Goerigk, *J. Comput. Chem.*, 2011, 32, 1456-1465.

[8] V. Wang, N. Xu, J.-C. Liu, G. Tang, W.-T. Geng, *Comput. Phys. Commun.*, 2021, 267, 108033.

[9] L. Gao, X. Cui, Z. Wang, C. D. Sewell, Z. Li, S. Liang, M. Zhang, J. Li, Y. Hu and Z. Lin, *Proc. Natl. Acad. Sci. U. S. A.*, 2021, 118, e2023421118.

[10] X. Ding, R. Jiang, J. Wu, M. Xing, Z. Qiao, X. Zeng, S. Wang and D. Cao, *Adv Funct Materials*, 2023, 33, 2306786.

[11] W.-Y. Fu, Y.-X. Lin, M.-S. Wang and Y.-S. Wei, *Rare Met.*, 2022, 41, 3069-3077.

[12] Y. Yang, H. Meng, C. Kong, S. Yan, W. Ma, H. Zhu, F. Ma, C. Wang, Z. Hu, *J. Colloid. Interf. Sci.*, 2021, 599, 300-312.

[13] X. Hou, H. Zhou, M. Zhao, Y. Cai and Q, Wei, *ACS Sustain. Chem. Eng.*, 2020, 8, 5724-5733.

[14] X. Jiang, H. Jang, S. Liu, Z. Li, M. G. Kim, C. Li, Q. Qin, X. Liu and J. Cho,

Angew. Chem. Int. Ed., 2021, 60, 4110–4116.

[15] S. Kim, S. Ji, H. Yang, H. Son, H. Choi, J. Kang and O. L. Li, *Appl. Catal., B*, 2022, 310, 121361.

[16] Z. Li, X. Lin, W. Xi, M. Shen, B. Gao, Y. Chen, Y. Zheng and B. Lin, *Appl. Surf. Sci.*, 2022, 593, 153446.

[17] G. Yasin, S. Ibraheem, S. Ali, M. Arif, S. Ibrahim, R. Iqbal, A. Kumar, M. Tabish, M. A. Mushtaq, A. Saad, H. Xu and W. Zhao, *Mater. Today Chem.*, 2022, 23, 100634.

[18] Z. Cai, L. Xu, Y. Zhou, L. Gao, X. An, X. Ma, Y. Ma, J. Liu, X. Li and K. Tang, *Int. J. Hydrogen. Energ.*, 2024, 82, 559–566.

[19] S. Wang, D. Yuan, S. Sun, S. Huang, Y. Wu, L. Zhang, S. X. Dou, H. K. Liu, Y. Dou and J. Xu, *Small*, 2024, 20, 2311770.

[20] S. Sun, C. Zhang, M. Ran, Y. Zheng, C. Li, Y. Jiang and X. Yan, *Int. J. Hydrogen. Energ.*, 2024, 63, 133–141.

[21] M. Afaq, M. Shahid, I. Ahmad, S. Yousaf, A. Alazmi, M. H. H. Mahmoud, I. H. El Azab and M. F. Warsi, *RSC Adv.*, 2023, 13, 19046–19057.

[22] C. V. M. Inocêncio, J. Rousseau, N. Guignard, C. Canaff, S. Morisset, T. W. Napporn, C. Morais and K. B. Kokoh, *Int. J. Hydrogen. Energ.*, 2023, 48, 26446–26460.

[23] C. Zhang, Y. Liu, J. Wang, W. Li, Y. Wang, G. Qin and Z. Lv, *Appl. Surf. Sci.*, 2022, 595, 153532.

[24] L. Qin, Q. Zheng, J. L. Liu, M. Zhang, M. Zhang and H. Zheng, *Mater. Chem. Front.*, 2021, 5, 7833–7842.